

SoC: Semantic Orthogonal Calibration for Test-Time Prompt Tuning

Leo Filliou^{1*}Omprakash Chakraborty²Ismail Ben Ayed²Paul-Henry Cournède¹Stergios Christodoulidis¹Maria Vakalopoulou¹Jose Dolz²¹ MICS, CentraleSupélec, Université Paris-Saclay, France² LIVIA, ILLS, ÉTS Montréal, Canada

Abstract

With the increasing adoption of vision-language models (VLMs) in critical decision-making systems such as healthcare or autonomous driving, the calibration of their uncertainty estimates becomes paramount. Yet, this dimension has been largely underexplored in the VLM test-time prompt-tuning (TPT) literature, which has predominantly focused on improving their discriminative performance. Recent state-of-the-art advocates for enforcing full orthogonality over pairs of text prompt embeddings to enhance separability, and therefore calibration. Nevertheless, as we theoretically show in this work, the inherent gradients from fully orthogonal constraints will strongly push semantically related classes away, ultimately making the model overconfident. Based on our findings, we propose Semantic Orthogonal Calibration (SoC), a Huber-based regularizer that enforces smooth prototype separation while preserving semantic proximity, thereby improving calibration compared to prior orthogonality-based approaches. Across a comprehensive empirical validation, we demonstrate that SoC consistently improves calibration performance, while also maintaining competitive discriminative capabilities.

1. Introduction

Pre-trained vision-language models (VLMs) [39, 49], built on millions of image-text pairs, have shown strong potential for capturing broad visual semantics and enabling generalization across a wide range of downstream vision tasks [39]. Yet, when deployed in real-world environments, these models inevitably confront the challenge of out-of-distribution data, for instance, in the form of tasks involving novel, unseen categories or domain shifts. This mismatch often undermines model generalization and scalability, particularly in scenarios where labeled data on the new task is scarce.

* Work done during an internship at ILLS.

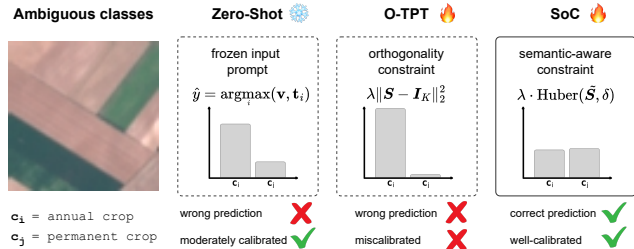


Figure 1. **Motivation for SoC.** With O-TPT, ambiguity inherent to the class semantics is lost due to the aggressive orthogonality constraint, leading to artificially high confidence, even when predictions are incorrect. Let us take this image as an example, whose correct class is “annual crop land”, and whose closest semantic class across all categories is “permanent crop land”. The zero-shot CLIP prediction incorrectly classifies the image, but its prediction remains uncertain, as the softmax for those two closely related categories remains close. In contrast, due to its orthogonality constraints, O-TPT [41] pushes the text class prototypes apart, making the model become more confident, even if the prediction is wrong. Our proposed **SoC** addresses this issue with a smoother orthogonality enforcement.

A simple solution consists in leveraging the zero-shot transferability of VLMs through carefully hand-crafted textual prompts, such as “a photo of a [CLASS]”, which does not require labeled data of the target class. While effective, manual prompt design often relies on domain-specific heuristics and may fail to generalize across diverse tasks. To address this drawback, test-time prompt tuning (TPT) [42] has emerged as a compelling alternative, enabling the optimization of textual prompts at inference without requiring labeled data and retraining. In particular, TPT learns prompt vectors via gradient descent, adaptively refining them using solely unlabeled test samples. By minimizing the entropy of the prediction distribution as a self-supervised signal, TPT allows VLMs, such as CLIP [39], to better align with novel tasks and unseen class semantics at

test time. Nevertheless, its reliance on entropy minimization as the only objective function induces overconfident predictions [33, 51], raising critical concerns about the reliability of VLMs. This is particularly important given the growing adoption of VLMs in real-world, safety-critical decision systems such as healthcare [15, 43], autonomous vehicles [14, 36], or video-surveillance [20], where the calibration of their uncertainty estimates becomes crucial.

To mitigate these limitations, calibration-oriented variants of TPT have been proposed, notably C-TPT [51] and O-TPT [41]. These approaches extend the original TPT paradigm by explicitly addressing the overconfidence induced by entropy minimization, encouraging dispersion between pairwise textual features. C-TPT [51] introduces a regularization objective that spreads textual embeddings away from their centroid. Nevertheless, it treats dispersion as a proxy for calibration, which limits the control over prototype geometry and semantic coherence. O-TPT [41], in contrast, operates directly on the geometry of the class prototype manifold, enforcing pairwise orthogonality between the class text embeddings. Although this improves separation, the strong repulsion for semantically similar (i.e., collinear) prototypes may actually be detrimental when the similarity reflects meaningful semantic overlap. For example, classes like *dog* and *puppy* are expected to be close in both image and text embedding spaces. Forcing such prototypes toward orthogonality disrupts the learned manifold and risks over-separating classes that should remain geometrically close. Furthermore, as we will demonstrate both analytically and empirically, the strong repulsion derived from full orthogonality results in systematic increases in confidence, which deteriorates model calibration, particularly for semantically similar categories. Based on these observations, the three key contributions of this study are:

- We introduce Semantic Orthogonal Calibration (SoC), a Huber-based regularizer for TPT, which yields smoother gradients than the full orthogonality constraints used in prior work (Fig. 1). While both induce systematic distortions in the embedding space, our formulation caps the repulsion for highly similar pairs, thereby better preserving semantic structure among related classes and mitigating the over-separation effects of strict orthogonality.
- We derive a *lower bound on the confidence* that links worst-case class similarity μ to prediction uncertainty, revealing how geometric repulsion influences calibration. This analysis shows that full orthogonality aggressively reduces μ , even for semantically correlated categories, leading to high confidence increase and degraded calibration. In contrast, the proposed regularizer applies gentler repulsion to high-similarity pairs, avoiding excessive confidence increases and better preserving semantic proximity, which ultimately yields better calibration.
- Comprehensive experiments across diverse benchmarks

on fine-grained classification and natural domain shifts demonstrate the superiority of our approach. SoC consistently improves calibration metrics over state-of-the-art baselines, while maintaining highly competitive discriminative performance, showing strong generalization across different backbones and diverse initial text prompts.

2. Related Work

Prompt tuning vision-language models. Vision-language models were introduced with CLIP [39] as a way of jointly training a vision and textual encoder to encode image-text pairs in a joint ℓ_2 -normalized space. These models are trained in a contrastive manner to maximize cosine similarity between positive pairs while minimizing it for negative pairs. The following works have built upon this pipeline, and explored various aspects such as scaling the dataset ([13]), exploring architectural choices and feature space fusion ([18, 30]), and the integration with large language models ([1, 19, 23]). One important feature of VLMs is their strong zero-shot performance, which enables them to classify input images given a text prompt and the class names. The image is classified using the highest cosine similarity between its embedding and the class embeddings. Prompt tuning allows to adapt the input prompt of a frozen VLM to a target task, using a limited number of samples (i.e., few-shot setting). CoOp [56] was introduced as a way to replace hand-crafted prompts with learnable prompts, which was later extended with CoCoOp [55] to include input-adaptive prompts. KgCoOp [7] builds upon CoOp, improving its generalizability to new classes by reducing the discrepancy between the hand-crafted and the learned prompt. Test-time prompt tuning (TPT) [27] shows that learning the input prompt at test-time (i.e., zero-shot setting) can increase the performance of the zero-shot classification in VLMs. Given an input test image and applying a batch of augmented views, the input prompt is updated in a single step of gradient descent by using the cross-entropy of the average prediction.

Calibrating modern neural networks. Model calibration has gained increasing popularity, where mainly post-processing [6, 50, 54] and training-time [21, 22, 31, 32, 38] approaches have emerged. In particular, temperature scaling [6] and its enhanced adaptive variants [50, 54] artificially increase the entropy of network predictions post hoc, whereas training-based methods typically aim to maximize the entropy of softmax outputs either explicitly [3, 38] or implicitly [31, 32] during training. Some other training-based approaches further incorporate penalty-based objectives into the primary loss function to regulate the separation between logits [21, 22]. Furthermore, data augmentation methods, such as Mixup [53], CutMix [52], and AugMix [9], train deep models on mixed samples to mitigate overconfident predictions.

Calibrating vision-language models. With the rapid rise of VLMs and their growing adoption in safety-critical applications, recent works have begun to explicitly address the uncertainty in their predictions. In particular, most of these approaches have focused on either full fine-tuning [25, 35, 45, 47] or few-shot learning [29] settings, which both require labeled samples, differing from the scenario studied in this work. SaLS [33] exposed that while most of the adaptation approaches enhance accuracy, they do it at the cost of degrading zero-shot calibration, and proposed an unsupervised logit normalization strategy to calibrate VLMs across different labeled regimes, including test-time prompt tuning. Closely related to our work, C-TPT [51] introduces a dispersion-based loss that encourages text embeddings to spread away from the class centroids, enhancing inter-class separability. While this improves diversity, it may underperform in complex scenarios due to limited utilization of the embedding space. O-TPT [41] builds on these weaknesses and enforces full orthogonality between the prompt class prototypes. In contrast, our approach introduces a smoother regularization mechanism that respects semantic proximity, avoiding the rigid separation imposed by full orthogonality, yet making more efficient use of the embedding space than dispersion-based methods like C-TPT.

3. Preliminaries

We first formally define the setting for VLM zero-shot classification before introducing the baseline methods.

3.1. Problem setting

A pretrained VLM consists of a vision encoder $f_\theta(\cdot)$ and a textual encoder $f_\phi(\cdot)$, which generate the image embedding $\mathbf{v} = f_\theta(\mathbf{x}) \in \mathbb{R}^d$ and the class prototypes $\mathbf{t}_k \in \mathbb{R}^d$, respectively. The class prototypes are generated by feeding a text template to the text encoder, $\mathbf{t}_k = f_\phi("a photo of a [CLASS]").$ Note that we resort to CLIP as a prominent VLM in the literature, which embeds the image and text embeddings in an ℓ_2 -normalized space, i.e. $\|\mathbf{v}\| = \|\{\mathbf{t}_k\}_{k=1}^K\| = 1$, with K being the number of classes. Let us define the logits and softmax probabilities:

$$\mathbf{z}_k = \alpha \mathbf{v}^\top \mathbf{t}_k, \quad \mathbf{p}_k(\mathbf{v}) = \frac{\exp(\mathbf{z}_k)}{\sum_{j=1}^K \exp(\mathbf{z}_j)},$$

where $\mathbf{z} = (z_k)_{1 \leq k \leq K}$, $\mathbf{p} = (p_k)_{1 \leq k \leq K}$, and $\alpha = \frac{1}{T}$, with T being the temperature scaling value controlling the shape of the softmax distributions, learned during pretraining [39].

We define $\mathbf{E} \in \mathbb{R}^{K \times d}$ as the matrix that contains all class prototypes. In addition, given that prototypes are unit norm, $\mathbf{S} = \mathbf{E}\mathbf{E}^\top$ defines the cosine similarity, where $s_{ij} = \mathbf{t}_i^\top \mathbf{t}_j$ is the cosine similarity between the class prototypes of classes i and j .

3.2. Relevant approaches

TPT [27]. Test-Time Prompt Tuning (TPT) optimizes the input text prompts by resorting to a cross entropy loss:

$$\mathcal{L}_{\text{TPT}} = - \sum_{k=1}^K \tilde{p}_k(\mathbf{v}) \log \tilde{p}_k(\mathbf{v}),$$

where, for a given test image \mathbf{x} , and its corresponding embedding \mathbf{v} , $\tilde{p}_k(\mathbf{v})$ is the average softmax probability across N augmentations, for the k -th class, thresholding to only keep the most confident predictions:

$$\tilde{p}_k(\mathbf{v}) = \frac{1}{\rho N} \sum_{n=1}^N \mathbb{1}(\mathcal{H}(p_k) \geq \tau) p_k(\mathcal{A}_n(\mathbf{v})),$$

with $\mathcal{A}_n(\mathbf{v})$ corresponding to the visual embedding of the image augmented with the n -th augmentation, and τ is the ρ -percentile of the entropy \mathcal{H} of N augmented views ranked from low to high.

C-TPT [51]. Based on TPT, C-TPT introduces a regularization term to maximize the distance between the text prototypes and their centroid:

$$\mathcal{L}_{\text{C-TPT}} = \mathcal{L}_{\text{TPT}} - \lambda \cdot \frac{1}{K} \sum_{k=1}^K \|\bar{\mathbf{t}} - \mathbf{t}_k\|_2,$$

where $\bar{\mathbf{t}} = \frac{1}{K} \sum_k \mathbf{t}_k$ is the centroid of textual embeddings.

O-TPT [41]. In a similar approach, O-TPT regularizes the TPT loss by adding a term that forces full orthogonality across pairs of text class prototypes.

$$\mathcal{L}_{\text{O-TPT}} = \mathcal{L}_{\text{TPT}} + \lambda \|\mathbf{S} - \mathbf{I}_K\|_2^2,$$

with \mathbf{I}_K denoting the identity matrix of dimension K , which removes the diagonal terms of the \mathbf{S} matrix.

3.3. Limitations of O-TPT

Despite the performance gains compared to C-TPT [51], O-TPT exhibits several limitations. In particular, full orthogonality imposes a quadratic penalty on pairwise similarity. This means that highly similar pairs are forced apart more aggressively than less similar ones. While this behaviour is initially sought, as it promotes separation, it can be sub-optimal for semantically correlated classes, i.e., those that are expected to have geometrical proximity due to conceptual overlap. For instance, consider the classes *annual crop land* and *permanent crop land*. These categories are naturally close in both image and text embedding manifolds, and their similarity reflects meaningful semantic structure. Under full orthogonality, their high similarity triggers strong repulsion, pushing them apart even though their proximity is desirable. Fig. 2 perfectly illustrates this, by showing how O-TPT makes overconfident predictions in classes that are semantically very close (i.e., with high zero-shot similarity).

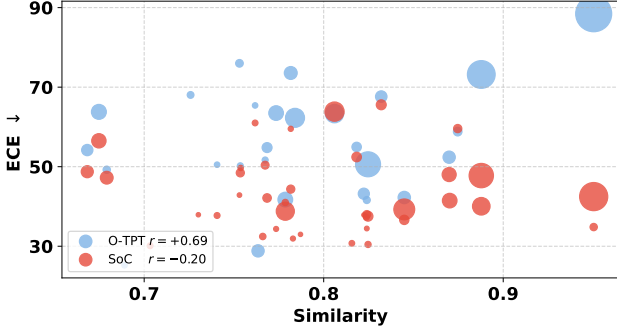


Figure 2. **ECE per class pair as a function of the zero-shot cosine similarity.** We compute the ECE for the wrong predictions across each class pair (i.e., the model predicted class i when the label was class j) and analyze the relation with the zero-shot similarity between both classes on EuroSAT. For classes with high initial semantic similarity, O-TPT is overconfident, caused by the underlying drawbacks of enforcing orthogonality across all pairs. Circle size indicates the number of samples in each (i, j) pair.

4. Our proposed SoC regularizer

Building on the above observations, we propose to enforce class prototype separation in a smoother manner, with a regularizer that respects semantic proximity. Specifically, we resort to the Huber loss [12], which is quadratic near zero but transitions to linear for larger residuals, preventing steep gradient growth for semantically similar pairs and making it a natural choice for our regularizer.

Given a margin $\delta \in [0, 1]$, we define our prompt tuning regularizer as:

$$\mathcal{L}_{\text{Huber}}(s, \delta) = \begin{cases} \frac{s^2}{2} & \text{if } s \leq \delta \\ \delta(s - \frac{\delta}{2}) & \text{otherwise,} \end{cases}$$

which is integrated into the whole learning objective:

$$\mathcal{L}_{\text{SoC}} = \mathcal{L}_{\text{TPT}} + \lambda \cdot \frac{2}{K(K-1)} \sum_{i < j} \mathcal{L}_{\text{Huber}}(s_{ij}, \delta),$$

with $\frac{K(K-1)}{2}$ denoting the number of elements in the lower triangle of the \mathbf{S} matrix.

4.1. Confidence bound under cosine coherence

We next formalize how the degree of prototype similarity directly controls the confidence floor of the softmax distribution. Let $i^* = \arg \max_i z_i$, and define the softmax confidence as:

$$p_{\max}(\mathbf{v}) = \max_i p_i(\mathbf{v}) = \frac{1}{1 + \sum_{j \neq i^*} \exp(-\Delta z_{i^*j}(\mathbf{v}))},$$

where the logit gap can be formally defined as:

$$\Delta z_{i^*j}(\mathbf{v}) = z_{i^*} - z_j = \alpha \mathbf{v}^\top (\mathbf{t}_{i^*} - \mathbf{t}_j).$$

Then, for any set of K classes ($K \geq 2$), let us define the *cosine coherence* of the set as:

$$\mu \triangleq \max_{i \neq j} \mathbf{t}_i^\top \mathbf{t}_j \in [0, 1]^1.$$

Proposition 1 (Confidence floor via cosine coherence). *For any unit vector \mathbf{v} , the confidence of the prediction satisfies*

$$p_{\max}(\mathbf{v}) \geq \frac{1}{1 + (K-1) \exp(-\alpha(1-\mu))}. \quad (1)$$

The proof is deferred to the Appendix Section A.

4.2. First-order analysis

To understand how orthogonality regularization influences model confidence and calibration, we analyze the immediate effect of a single gradient step on the geometry of the prototype space (note that O-TPT [41], similarly to other TPT-based methods, performs only one gradient step over text embeddings). Specifically, we investigate how the worst-case similarity $\mu = \max_{i \neq j} s_{ij}$ evolves under full orthogonality (O-TPT) and the proposed Huber-style regularizer. This quantity directly controls the softmax confidence lower bound (Proposition 1), and its reduction is often interpreted as a proxy for improved separation. However, the mechanism by which μ is reduced has important implications for semantic preservation and calibration.

Let us consider only a single gradient step of size $\eta > 0$, use the first-order approximation, and assume the worst-case similarity $\mu = \max_{i \neq j} s_{ij}$ is attained by the dominant pair in the set. We now formalize the update dynamics. A single gradient step of size η yields the updated prototypes $\mathbf{t}'_i = \mathbf{t}_i - \eta \nabla_{\mathbf{t}_i}$, and updated similarity $s'_{ij} = (\mathbf{t}'_i)^\top \mathbf{t}'_j$. Thus, the first-order pairwise similarity shift, which captures how the cosine similarity between class prototypes \mathbf{t}_i and \mathbf{t}_j evolves, can be defined as:

$$\Delta s_{ij} \equiv s'_{ij} - s_{ij} \approx -\eta (\mathbf{t}_j^\top \nabla_{\mathbf{t}_i} + \mathbf{t}_i^\top \nabla_{\mathbf{t}_j}), \quad (2)$$

where the last approximation follows from a first-order Taylor expansion, with the $\mathcal{O}(\eta^2)$ term ignored, as it is negligible under small-step first-order dynamics.

Full orthogonality leads to the following gradient, $\nabla_{\mathbf{t}_i}^{\text{O-TPT}} = 2 \sum_{k \neq i} s_{ik} \mathbf{t}_k$, whereas the gradient from the proposed Huber-style regularized is:

$$\nabla_{\mathbf{t}_i}^{\text{Huber}} = \sum_{k \neq i} g_\delta(s_{ik}) \mathbf{t}_k, \text{ where } g_\delta(s) = \begin{cases} s, & s \leq \delta, \\ \delta, & s > \delta. \end{cases}$$

For analytical clarity, we approximate the gradient by retaining only the dominant pair (i, j) , i.e., the neighbors attaining the highest similarity. Specifically:

$$\nabla_{\mathbf{t}_i}^{\text{O-TPT}} \approx 2 s_{ij} \mathbf{t}_j, \quad \nabla_{\mathbf{t}_j}^{\text{O-TPT}} \approx 2 s_{ij} \mathbf{t}_i,$$

¹We assume CLIP-style class embeddings, which are unit-normalized and yield non-negative pairwise cosine similarities.

and

$$\nabla_{\mathbf{t}_i}^{\text{Huber}} \approx g_\delta(s_{ij}) \mathbf{t}_j, \quad \nabla_{\mathbf{t}_j}^{\text{Huber}} \approx 2g_\delta(s_{ij}) \mathbf{t}_i.$$

Note that this simplification still highlights the repulsion effect without altering the qualitative behavior of the update (the exact derivation considering all pairs is derived in Appendix B). Using the first-order update rule (Eq. 2):

$$\begin{aligned} \Delta s_{ij}^{\text{O-TPT}} &\approx -\eta(\mathbf{t}_j^\top (2s_{ij}\mathbf{t}_j) + \mathbf{t}_i^\top (2s_{ij}\mathbf{t}_j)), \\ &\approx -2\eta s_{ij}(\|\mathbf{t}_j\|^2 + \|\mathbf{t}_i\|^2) \\ &\approx -4\eta s_{ij}. \end{aligned} \quad (3)$$

Similarly, for the proposed Huber-based regularizer:

$$\begin{aligned} \Delta s_{ij}^{\text{Huber}} &\approx -\eta(\mathbf{t}_j^\top (g_\delta(s_{ij})\mathbf{t}_j) + \mathbf{t}_i^\top (g_\delta(s_{ij})\mathbf{t}_j)), \\ &\approx -\eta g_\delta(s_{ij})(\|\mathbf{t}_j\|^2 + \|\mathbf{t}_i\|^2) \\ &\approx -2\eta g_\delta(s_{ij}) = \begin{cases} -2\eta s_{ij}, & s_{ij} \leq \delta, \\ -2\eta \delta, & s_{ij} > \delta. \end{cases} \end{aligned} \quad (4)$$

Then, after one step, considering $\mu = s_{ij}$, and the gradients in Eq. (3) and (4):

$$\begin{aligned} \mu'_{\text{O-TPT}} &\approx (1 - 4\eta)\mu, \\ \mu'_{\text{Huber}} &\approx \begin{cases} (1 - 2\eta)\mu, & \mu \leq \delta, \\ \mu - 2\eta\delta, & \mu > \delta. \end{cases} \end{aligned}$$

The behavior of the proposed Huber regularizer depends on whether μ lies below or above the threshold δ :

- When $\mu \leq \delta$: the Huber gradient yields a similarity update of $\mu'_{\text{Huber}} = (1 - 2\eta)\mu$. In contrast, O-TPT applies a stronger repulsion, resulting in $\mu'_{\text{O-TPT}} = (1 - 4\eta)\mu$. Thus, even in the low-similarity regime, O-TPT contracts μ more aggressively than Huber.
- When $\mu > \delta$: the Huber update becomes capped ($\mu'_{\text{Huber}} = \mu - 2\eta\delta$), while O-TPT continues to scale with μ ($\mu'_{\text{O-TPT}} = (1 - 4\eta)\mu$).

Comparing both, we find that:

$$\mu'_{\text{O-TPT}} < \mu'_{\text{Huber}} \quad \text{iff} \quad 4\mu > 2\delta,$$

which holds whenever $\mu > \delta$. This confirms that O-TPT consistently yields a sharper one-step reduction than the proposed Huber regularizer in worst-case similarity, regardless of the threshold δ .

Corollary 1 (Confidence increases under full orthogonality). *Let $\mu = \max_{i \neq j} s_{ij}$ denote the worst-case similarity between class prototypes, and let $p_{\max}(\mathbf{v})$ be the softmax confidence lower bound as defined in Proposition 1. Then, under a single gradient step of size η , full orthogonality (O-TPT [41]) yields a strictly lower worst-case similarity than Huber-style regularization:*

$$\mu'_{\text{O-TPT}} < \mu'_{\text{Huber}},$$

and therefore a strictly higher confidence bound:

$$p_{\max}^{\text{O-TPT}}(\mathbf{v}) > p_{\max}^{\text{Huber}}(\mathbf{v}).$$

This result highlights the geometric mechanism by which O-TPT inflates confidence more aggressively than the proposed Huber-based regularizer, SoC.

5. Experiments

5.1. Experimental setup

Datasets. Building upon previous works [27, 41, 51], we first evaluate our approach on a comprehensive benchmark that encompasses **11 diverse image classification datasets**, including: two generic-objects datasets (ImageNet [5], Caltech101 [17]), five fine-grained datasets (OxfordPets [37], StanfordCars [16], Flowers102 [34], Food101 [2], FGVC-Aircraft [26]), a scene recognition dataset (SUN397 [48]), an action recognition dataset (UCF101 [44]), a texture dataset (DTD [4]), and a satellite image dataset (EuroSAT [8]). Furthermore, we also evaluate SoC on the four variants of the popular ImageNet, namely ImageNet-A [11], ImageNet-v2 [40], ImageNet-R [10], and ImageNet-Sketch [46]. Further datasets details are presented in Appendix C.

Baselines. We use TPT [27] as the main baseline, whose learning objective is solely focused on improving classification accuracy. Furthermore, we include C-TPT [51] and O-TPT [41] as relevant concurrent methods that have been proposed to enhance TPT. We conduct the experiments under identical settings across methods to ensure a fair comparison.

Implementation details. We use ViTs of different sizes as backbone networks (ViT-L/14 and ViT-B/16, with ViT-L/14 used across experiments, unless otherwise stated), as they have been shown to be better calibrated than CNNs [28], and thus represent a more realistic scenario. Following [41, 51], prompts are initialized as “a photo of a [CLASS]” and optimized using AdamW [24] over a single gradient step, and a learning rate of 0.005. The batch size is set to 64 across all experiments (corresponding to 64 augmentations of each image), similar to [41]. All remaining settings strictly adhere to the configuration in [41, 51]. Further details are provided in Appendix Section D.

Evaluation metrics. To evaluate the classification performance, we rely on accuracy. Then, in order to compare the calibration with C-TPT and O-TPT, we report the expected calibration error (ECE). Given a test set of size M with visual embeddings $V = \{\mathbf{v}_1, \dots, \mathbf{v}_M\}$ with labels $Y = \{y_1, \dots, y_M\}$, and class prototypes $T = \{\mathbf{t}_1, \dots, \mathbf{t}_K\}$. Let us define by $\gamma(\mathbf{v}, y) = \mathbb{1}(\arg \max_j (\mathbf{v}^\top \mathbf{t}_j) = y)$ the binary operator for determining correct sample-wise classification, and by $\epsilon(\mathbf{v}, b) = \mathbb{1}(\text{softmax}(\max_j (\mathbf{v}^\top \mathbf{t}_j)) \in b)$ the binary operator indicating if the maximum softmax for

Table 1. **Benchmark with the ViT-L/14 backbone.** Accuracy and ECE across 11 datasets compared with four baseline methods. Green and red indicate positive and negative changes with respect to state-of-the-art O-TPT [41], respectively.

	ImgNet	DTD	Flowers	Food101	SUN397	Aircraft	Pets	Caltech	UCF101	EuroSAT	Cars	Average	
Accuracy	Zero-Shot	73.5	52.4	76.2	88.6	67.7	29.9	93.1	95.1	73.8	55.0	76.8	71.1
	TPT _{NeurIPS'22}	75.6	55.3	76.3	89.0	70.2	31.8	93.6	95.5	74.9	51.9	77.8	72.0
	C-TPT _{ICLR'24}	75.0	55.1	76.5	88.9	70.1	30.9	94.1	95.5	75.2	54.0	77.5	72.1
	O-TPT _{CVPR'25}	73.2	54.6	76.4	88.6	68.9	30.0	93.8	95.3	74.5	53.6	76.7	71.4
	SoC (Ours)	74.5_{+1.3}	54.4_{-0.2}	77.0_{+0.6}	88.9_{+0.3}	69.5_{+0.6}	30.9_{+0.9}	93.9_{+0.1}	95.6_{+0.3}	74.9_{+0.4}	58.3_{+4.7}	77.0_{+0.3}	72.3_{+0.9}
ECE	Zero-Shot	2.9	10.3	4.3	1.8	3.3	10.3	2.8	3.7	5.6	6.9	3.9	5.1
	TPT _{NeurIPS'22}	14.8	25.0	15.0	6.2	17.2	28.8	3.7	2.4	17.7	25.8	7.1	14.9
	C-TPT _{ICLR'24}	10.5	18.3	11.1	3.3	13.5	21.4	1.0	0.9	11.1	17.3	1.4	10.0
	O-TPT _{CVPR'25}	5.5	13.8	7.0	2.8	7.6	16.8	1.4	2.0	8.5	17.7	2.2	7.7
	SoC (Ours)	7.2_{+1.7}	10.9_{-2.9}	5.3_{-1.7}	2.1_{-0.7}	7.2_{-0.4}	12.7_{-4.1}	0.5_{-0.9}	1.3_{-0.7}	6.5_{-2.0}	3.2_{-14.5}	2.2_{-0.0}	5.4_{-2.3}

\mathbf{v} falls in bin b .

$$\text{ECE}(V, Y, T) = \frac{1}{|B|} \sum_{b_i \in B} n_i |\gamma(\mathbf{v}_m, y_m) \cdot \epsilon(\mathbf{v}_m, b_i) - \bar{b}_i|$$

with B the bins into which to split the confidence scores, $n_i = \sum_{\mathbf{v}_m} \epsilon(\mathbf{v}_m, b_i)$ the number of elements in the i -th bin, and \bar{b}_i the median bin value.

5.2. Results

Performance on fine-grained classification tasks. Tab. 1 reports the results across 11 fine-grained classification datasets for the different approaches. We can observe that, while SoC improves the overall classification performance compared to previous TPT-based methods, it also yields the best calibrated prediction, whose mean ECE differences range from 2.3 (compared to O-TPT) to 9.5 with respect to the original TPT method. Particularly, compared to the previous state-of-the-art O-TPT, SoC achieves the best ECE scores in all but one dataset, showing its robustness across multiple datasets. Furthermore, it is noteworthy to mention that, from a calibration standpoint, our approach performs on par with zero-shot, which has been shown in recent literature to provide the best calibration [33].

In addition to these numerical results, we depict reliability diagrams (Fig. 3) across three representative datasets, which can be used to show not only the extent of miscalibration, but also the direction of the miscalibration, i.e., whether the model is systematically overconfident or underconfident. Looking closely at these plots, they reveal that O-TPT exhibits pronounced overconfidence, with predicted probabilities consistently exceeding observed accuracies. In contrast, SoC yields flatter reliability curves that more closely follow the diagonal, indicating better alignment between confidence and accuracy. This reduction directly translates into lower ECE scores, and supports the theoretical findings presented in Corollary 1, which show that full orthogonality increases the confidence floor more aggressively than our Huber-like regularizer, virtually increasing confidence.

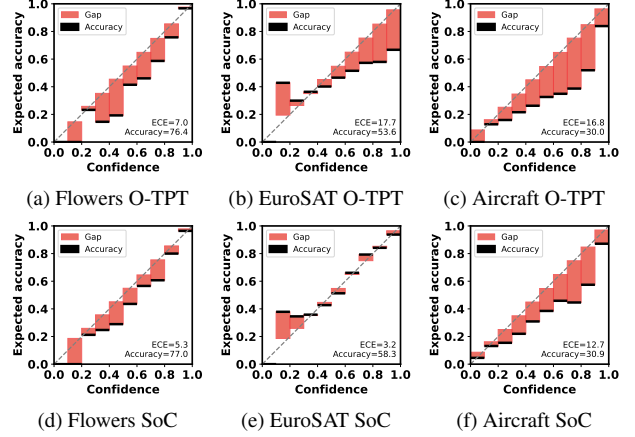


Figure 3. **Reliability diagrams of O-TPT vs SoC.** Plots showing the calibration error across the Flowers102, EuroSAT and FGVC Aircraft datasets for O-TPT (top row) and SoC (bottom row).

Robustness under natural distributional drifts. Tab. 2 presents the results across the four different variants of ImageNet, which present a distributional drift. In particular, we can observe that while performing on par with O-TPT in terms of accuracy, it decreases the ECE by 1.5. Similarly, even though TPT and C-TPT yield higher accuracy, calibration metrics are substantially improved, e.g., 5.8 and 4.2, compared to TPT and C-TPT, respectively. These results align with the observations in O-TPT, where TPT and C-TPT achieved better discriminative performance, at the cost of large degradations in calibration. Together, these outcomes underscore the ability of our approach to adapt to natural distribution shifts while enhancing the uncertainty.

O-TPT confidence significantly increases in multi-step TPT. TPT-based approaches typically perform a single update of the prompts. Under this well-established scenario, and motivated by our analytical findings on confidence inflation under full orthogonality (*Proposition 1*, *Corollary 1*), we empirically investigate the impact of applying two gradient updates on calibration and performance, whose re-

Table 2. **Distribution shift (ViT-L/14 backbone).** Accuracy and ECE across four variants of the ImageNet dataset compared to the four compared baselines. Green and red indicate positive and negative changes with respect to O-TPT, respectively.

	-A	-v2	-R	-Sketch	Average
Accuracy	Zero-Shot	68.8	67.9	85.4	57.8
	TPT	73.9	70.0	87.8	59.7
	C-TPT	72.0	69.9	86.7	59.5
	O-TPT	71.3	69.0	86.0	58.8
	SoC (Ours)	70.4_{-0.9}	68.9_{-0.1}	86.8_{+0.9}	58.9_{+0.1}
ECE	Zero-Shot	3.9	3.9	2.5	7.4
	TPT	13.1	16.4	5.0	22.2
	C-TPT	11.7	14.6	3.5	20.4
	O-TPT	10.8	10.6	2.7	15.3
	SoC (Ours)	7.3_{-3.5}	10.4_{-0.2}	1.4_{-1.3}	14.4_{-0.9}

sults are shown in Fig. 4. While C-TPT, O-TPT, and SoC were all negatively impacted by performing an additional gradient update, the effect was much less pronounced on our method, particularly from a calibration standpoint. Indeed, while the ECE obtained by SoC degraded nearly 23% after a second gradient update, O-TPT calibration deteriorated by 39%, nearly twice as much. This behavior aligns with our first-order analysis (Section 4.2), which shows that full orthogonality induces sharper reductions in worst-case similarity μ per gradient step, leading to virtually increased confidence, even when unnecessary.

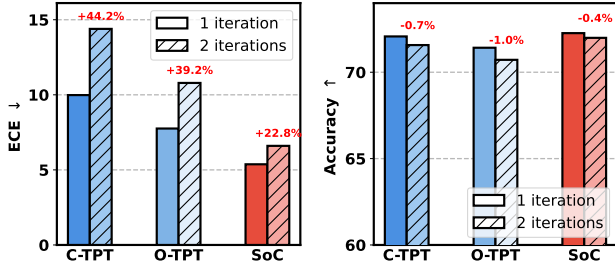


Figure 4. **ECE and accuracy for one and two gradient steps.** Standard one-step and two-step gradient updates for C-TPT, O-TPT, and SoC averaged across 11 datasets. Hatched bars indicate the result when applying two gradient updates over text prompts.

Robustness to backbone. To assess the robustness of our method across different backbone architectures, we extend our evaluation and include results using ViT-B/16. This comparison allows us to verify whether the calibration and alignment benefits inherent in our regularizer persist under smaller, less expressive models (Tab. 3). In particular, we observe a similar trend to that observed in the ViT-L/14 backbone, i.e., SoC outperforms state-of-the-art O-TPT in accuracy and ECE. Furthermore, it is interesting to note that, while SoC enhances the discriminative performance of zero-shot (ZS) predictions (+0.7 and +1.2), it maintains

highly comparable ECE scores across backbones (4.3 vs 4.2; 5.4 vs 5.1). This highlights the strong calibration properties of our approach, alongside with its ability to improve ZS performance.

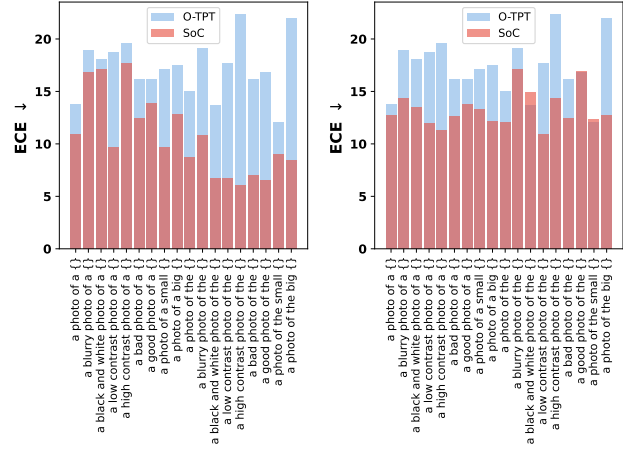


Figure 5. **Calibration sensitivity of O-TPT vs. SoC for various initial text prompts.** ECE on the DTD (left) and Aircraft (right) datasets for 18 different prompts from CLIP [39].

Calibration across prompt variability. Prompt initialization remains a critical factor in CLIP-based adaptation, as different textual templates can induce large variations in calibration. Fig. 5 depicts ECE across 18 CLIP text prompts for two different datasets. While both O-TPT and SoC exhibit sensitivity, an interesting observation is that our approach yields lower ECE across nearly all prompts. In other words, even though calibration still depends on prompt initialization, our regularizer typically limits the extreme overconfidence spikes characteristic of O-TPT. These results underscore that SoC delivers more reliable predictions than O-TPT, regardless of the chosen template.

Prompt initialization with CoOp. CoOp [56] is a prompt tuning method for VLMs, which can be used to optimize the initial prompt in a few-shot setting. As in O-TPT [41], we evaluate the prompt embeddings trained in a supervised manner, using k -shots, to evaluate the

Table 3. **Robustness to backbone.** Average accuracy and ECE across all 11 datasets for two sizes of ViTs. Differences with respect to O-TPT are highlighted in green.

	ViT-B/16		ViT-L/14	
	Acc.	ECE	Acc.	ECE
Zero-Shot	63.9	4.2	71.1	5.1
TPT	65.2	11.2	72.0	14.9
C-TPT	64.6	5.0	72.1	10.0
O-TPT	64.0	4.8	71.4	7.7
SoC (Ours)	64.6_{+0.6}	4.3_{-0.5}	72.3_{+0.9}	5.4_{-2.3}

calibration effectiveness of these prompts with SoC during test-time prompt tuning. Tab. 4 shows results when using CoOp-initialized prompts, trained for 2-shots and 4-shots. SoC keeps outperforming O-TPT both in terms of accuracy and calibration, even though the gap get smaller as the accuracy increases and the calibration error decreases.

Table 4. Effect of pretraining the prompts with CoOp. Results show the average across all 11 datasets for 2-shot and 4-shot pre-trained prompts using CoOp. Baseline represents using the non-CoOp-initialized prompts. Differences with respect to O-TPT are highlighted in green.

	Baseline	2-shots	4-shots
Accuracy			
TPT _{+CoOp}	72.0	76.0	80.2
C-TPT _{+CoOp}	72.1	74.1	78.3
O-TPT _{+CoOp}	71.4	72.9	76.6
SoC_{+CoOp (Ours)}	72.3_{+0.9}	75.2_{+2.3}	78.0_{+1.4}
ECE			
TPT _{+CoOp}	14.9	14.8	11.7
C-TPT _{+CoOp}	10.0	10.4	7.7
O-TPT _{+CoOp}	7.7	7.4	5.6
SoC_{+CoOp (Ours)}	5.4_{-2.3}	6.3_{-1.1}	5.4_{-0.2}

When the model is confident, how often is it correct? To further evaluate the reliability of our method, we report selective classification accuracy under varying confidence thresholds (Fig. 6). This setting reflects practical deployment scenarios where predictions are accepted only if the model’s confidence exceeds a predefined threshold, making calibration critical for safe decision-making. Across all thresholds, SoC consistently outperforms TPT, C-TPT, and O-TPT, achieving higher selective accuracy, with gaps often ranging between 5-10%. Notably, across all thresholds, our method matches the performance of the ZS baseline, despite being adapted on unlabeled test data. This indicates that our regularizer preserves semantic alignment while improving calibration. It is important to note that, even though ZS CLIP appears strong in this setting, it benefits from fixed, pretrained text embeddings that are not exposed to entropy minimization or adaptation-induced drift. However, as shown in prior experiments, it lacks flexibility and cannot adapt to domain-specific semantics. In contrast, our method retains the robustness of ZS while enabling task-specific adaptation, yielding superior performance at lower thresholds, where calibration plays a larger role in filtering uncertain predictions.

These results reinforce our core claim: *by limiting confidence increase and preserving semantic proximity, SoC enables reliable adaptation without sacrificing reliability.* This makes it especially suitable for real-world applications, where selective prediction is paramount.

Further improving SoC performance. SaLS [33] presented a simple, model-agnostic post-hoc strategy to enhance calibration of TPT, among other adaptation strate-

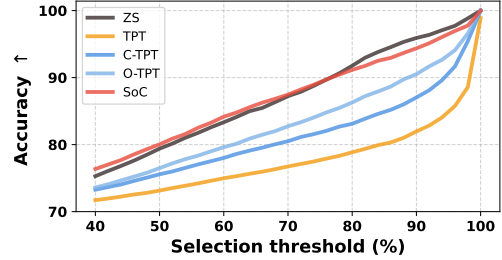


Figure 6. Selective accuracy across different thresholds. For each threshold, we select only the samples whose confidence (i.e., maximum of softmax) exceeds that value, and compute the accuracy on this subset.

gies. To assess the compatibility of our method with post-hoc calibration strategies, we apply SaLS to C-TPT, O-TPT, and SoC. These results, depicted in Fig. 7, demonstrate that SaLS often enhances the calibration results provided by our approach, showcasing its complementarity. Indeed, even when SaLS is applied across all methods, our approach remains the best calibrated across nearly all datasets. Last, it is noteworthy to highlight that the improvements from SaLS are notably smaller on our method, which indicates that the predictions from SoC are often already well-calibrated prior to post-hoc adjustment, demonstrating the stronger calibration capabilities of the proposed approach.

Additional experiments and results are presented in Appendix Section E.

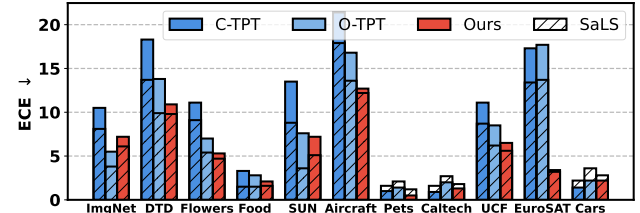


Figure 7. ECE with and without SaLS. ECE for C-TPT, O-TPT, and SoC with and without applying SaLS for further calibration.

6. Conclusion

In this work, we have shown that enforcing full orthogonality (i.e., O-TPT) in test-time prompt tuning, while intuitively appealing, systematically distorts semantic structure and inflates confidence, potentially amplifying miscalibration. This issue is particularly magnified in classes with high semantic similarity, which are naturally close in both image and text embedding manifolds. To address this limitation, we have presented **SoC**, which replaces the strong repulsion in O-TPT with a Huber-based regularizer that respects semantic proximity, yielding smoother prototype

geometry and improved calibration. To support our theoretical findings, comprehensive experiments across diverse datasets and backbones demonstrate that SoC consistently outperforms prior calibration-oriented TPT methods, while preserving competitive accuracy. We believe that our analysis on the impact of enforcing full orthogonality for highly similar pairs opens the door to more semantically-aware calibration methods for VLMs.

Acknowledgments. This work has benefited from state financial aid, managed by the Agence Nationale de Recherche under the investment program integrated into France 2030, project reference ANR-21-RHUS-0003. We acknowledge the support of the Natural Sciences and Engineering Research Council of Canada (NSERC). This work was granted access to the HPC resources of IDRIS under the allocation 2024-AD011014802R1 made by GENCI. The author gratefully acknowledges support from ILLS during the internship in which this work was conducted.

References

- [1] Jean-Baptiste Alayrac, Jeff Donahue, Pauline Luc, Antoine Miech, Iain Barr, Yana Hasson, Karel Lenc, Arthur Mensch, Katie Millicah, Malcolm Reynolds, Roman Ring, Eliza Rutherford, Serkan Cabi, Tengda Han, Zhitao Gong, Sina Samangooei, Marianne Monteiro, Jacob Menick, Sebastian Borgeaud, Andrew Brock, Aida Nematzadeh, Sahand Sharifzadeh, Mikolaj Binkowski, Ricardo Barreira, Oriol Vinyals, Andrew Zisserman, and Karen Simonyan. Flamingo: a visual language model for few-shot learning. In *Proceedings of the 36th International Conference on Neural Information Processing Systems*, Red Hook, NY, USA, 2022. Curran Associates Inc. [2](#)
- [2] Lukas Bossard, Matthieu Guillaumin, and Luc Van Gool. Food-101 – mining discriminative components with random forests. In *European Conference on Computer Vision*, 2014. [5, 3](#)
- [3] Jiacheng Cheng and Nuno Vasconcelos. Calibrating deep neural networks by pairwise constraints. In *Proceedings of the IEEE/CVF Conference on Computer Vision and Pattern Recognition*, pages 13709–13718, 2022. [2](#)
- [4] M. Cimpoi, S. Maji, I. Kokkinos, S. Mohamed, , and A. Vedaldi. Describing textures in the wild. In *IEEE Conference on Computer Vision and Pattern Recognition*, 2014. [5, 3](#)
- [5] Jia Deng, Wei Dong, Richard Socher, Li-Jia Li, Kai Li, and Li Fei-Fei. Imagenet: A large-scale hierarchical image database. In *2009 IEEE Conference on Computer Vision and Pattern Recognition*, pages 248–255, 2009. [5, 3](#)
- [6] Chuan Guo, Geoff Pleiss, Yu Sun, and Kilian Q. Weinberger. On calibration of modern neural networks. In *Proceedings of the 34th International Conference on Machine Learning - Volume 70*, page 1321–1330. JMLR.org, 2017. [2](#)
- [7] Changsheng Xu Hantao Yao, Rui Zhang. Visual-language prompt tuning with knowledge-guided context optimization. In *The IEEE/CVF Conference on Computer Vision and Pattern Recognition*, 2023. [2](#)
- [8] Patrick Helber, Benjamin Bischke, Andreas Dengel, and Damian Borth. Eurosat: A novel dataset and deep learning benchmark for land use and land cover classification. *IEEE Journal of Selected Topics in Applied Earth Observations and Remote Sensing*, 2019. [5, 3](#)
- [9] Dan Hendrycks, Norman Mu, Ekin D. Cubuk, Barret Zoph, Justin Gilmer, and Balaji Lakshminarayanan. Augmix: A simple data processing method to improve robustness and uncertainty. In *International Conference on Learning Representations (ICLR)*, 2020. [2](#)
- [10] Dan Hendrycks, Steven Basart, Norman Mu, Saurav Kadavath, Frank Wang, Evan Dorundo, Rahul Desai, Tyler Zhu, Samyak Parajuli, Mike Guo, Dawn Song, Jacob Steinhardt, and Justin Gilmer. The many faces of robustness: A critical analysis of out-of-distribution generalization. *ICCV*, 2021. [5, 3](#)
- [11] Dan Hendrycks, Kevin Zhao, Steven Basart, Jacob Steinhardt, and Dawn Song. Natural adversarial examples. In *Proceedings of the IEEE/CVF Conference on Computer Vision and Pattern Recognition (CVPR)*, pages 15262–15271, 2021. [5, 3](#)
- [12] Peter J. Huber. Robust estimation of a location parameter. *Annals of Mathematical Statistics*, 35(1):73–101, 1964. [4](#)
- [13] Chao Jia, Yinfai Yang, Ye Xia, Yi-Ting Chen, Zarana Parekh, Hieu Pham, Quoc V. Le, Yun-Hsuan Sung, Zhen Li, and Tom Duerig. Scaling up visual and vision-language representation learning with noisy text supervision. In *International Conference on Machine Learning*, 2021. [2](#)
- [14] Apoorv Khandelwal, Luca Weihs, Roozbeh Mottaghi, and Aniruddha Kembhavi. Simple but effective: CLIP embeddings for embodied AI. In *Proceedings of the IEEE/CVF Conference on Computer Vision and Pattern Recognition*, pages 14829–14838, 2022. [2](#)
- [15] Taha Koleilat, Hojat Asgariandehkordi, Hassan Rivaz, and Yiming Xiao. Biomedcoop: Learning to prompt for biomedical vision-language models. In *Proceedings of the Computer Vision and Pattern Recognition Conference*, pages 14766–14776, 2025. [2](#)
- [16] Jonathan Krause, Michael Stark, Jia Deng, and Li Fei-Fei. 3d object representations for fine-grained categorization. In *4th International IEEE Workshop on 3D Representation and Recognition (3dRR-13)*, Sydney, Australia, 2013. [5, 3](#)
- [17] Fei-Fei Li, Rob Fergus, and Pietro Perona. One-shot learning of object categories. *IEEE Transactions on Pattern Analysis and Machine Intelligence*, 2006. [5, 3](#)
- [18] Junnan Li, Ramprasaath R. Selvaraju, Akhilesh Deepak Gotmare, Shafiq Joty, Caiming Xiong, and Steven Hoi. Align before fuse: Vision and language representation learning with momentum distillation. In *NeurIPS*, 2021. [2](#)
- [19] Junnan Li, Dongxu Li, Caiming Xiong, and Steven C. H. Hoi. Blip: Bootstrapping language-image pre-training for unified vision-language understanding and generation. In *International Conference on Machine Learning*, 2022. [2](#)
- [20] Siyuan Li, Li Sun, and Qingli Li. CLIP-reID: exploiting vision-language model for image re-identification without concrete text labels. In *Proceedings of the AAAI conference on artificial intelligence*, pages 1405–1413, 2023. [2](#)

[21] Bingyuan Liu, Ismail Ben Ayed, Adrian Galdran, and Jose Dolz. The devil is in the margin: Margin-based label smoothing for network calibration. In *Proceedings of the IEEE/CVF Conference on Computer Vision and Pattern Recognition (CVPR)*, pages 80–88, 2022. 2

[22] Bingyuan Liu, Jérôme Rony, Adrian Galdran, Jose Dolz, and Ismail Ben Ayed. Class adaptive network calibration. In *Conference on Computer Vision and Pattern Recognition (CVPR)*, pages 16070–16079, 2023. 2

[23] Haotian Liu, Chunyuan Li, Qingyang Wu, and Yong Jae Lee. Visual instruction tuning, 2023. 2

[24] Ilya Loshchilov and Frank Hutter. Decoupled weight decay regularization. In *International Conference on Learning Representations (ICLR)*, 2019. 5

[25] Song-Lin Lv, Yu-Yang Chen, Zhi Zhou, Yu-Feng Li, and Lan-Zhe Guo. Contrast-aware calibration for fine-tuned CLIP: Leveraging image-text alignment. *arXiv preprint arXiv:2501.19060*, 2025. 3

[26] S. Maji, J. Kannala, E. Rahtu, M. Blaschko, and A. Vedaldi. Fine-grained visual classification of aircraft. Technical report, 2013. 5, 3

[27] Shu Manli, Nie Weili, Huang De-An, Yu Zhiding, Goldstein Tom, Anandkumar Anima, and Xiao Chaowei. Test-time prompt tuning for zero-shot generalization in vision-language models. In *NeurIPS*, 2022. 2, 3, 5

[28] Matthias Minderer, Josip Djolonga, Rob Romijnders, Frances Hubis, Xiaohua Zhai, Neil Houlsby, Dustin Tran, and Mario Lucic. Revisiting the calibration of modern neural networks. In *Advances in Neural Information Processing Systems*, pages 15682–15694. Curran Associates, Inc., 2021. 5

[29] Pablo Morales-Álvarez, Stergios Christodoulidis, Maria Vakalopoulou, Pablo Piantanida, and Jose Dolz. Bayesadapter: enhanced uncertainty estimation in CLIP few-shot adaptation. *International Journal of Computer Vision (IJCV)*, 2025. 3

[30] Norman Mu, Alexander Kirillov, David Wagner, and Saining Xie. Slip: Self-supervision meets language-image pre-training. In *Computer Vision – ECCV 2022*, pages 514–532. Springer International Publishing, 2022. 2

[31] Jishnu Mukhoti et al. Calibrating deep neural networks using focal loss. In *Advances in Neural Information Processing Systems (NeurIPS)*, 2020. 2

[32] Rafael Müller et al. When does label smoothing help? *NeurIPS*, 32, 2019. 2

[33] Balamurali Murugesan, Julio Silva-Rodriguez, Ismail Ben Ayed, and Jose Dolz. Robust calibration of large vision-language adapters. In *European Conference on Computer Vision (ECCV)*, 2024. 2, 3, 6, 8, 4, 5

[34] M-E. Nilsback and A. Zisserman. Automated flower classification over a large number of classes. In *Indian Conference on Computer Vision, Graphics and Image Processing*, 2008. 5, 3

[35] Changdae Oh, Hyesu Lim, Mijoo Kim, Dongyoon Han, Sangdoo Yun, Jaegul Choo, Alexander Hauptmann, Zhi-Qi Cheng, and Kyungwoo Song. Towards calibrated robust fine-tuning of vision-language models. *Advances in Neural Information Processing Systems*, 37:12677–12707, 2024. 3

[36] Chenbin Pan, Burhaneddin Yaman, Tommaso Nesti, Abhirup Mallik, Alessandro G Allievi, Senem Velipasalar, and Liu Ren. VLP: Vision language planning for autonomous driving. In *Proceedings of the IEEE/CVF Conference on Computer Vision and Pattern Recognition*, pages 14760–14769, 2024. 2

[37] O. M. Parkhi, A. Vedaldi, A. Zisserman, and C. V. Jawahar. Cats and dogs. In *IEEE Conference on Computer Vision and Pattern Recognition*, 2012. 5, 3

[38] Gabriel Pereyra et al. Regularizing neural networks by penalizing confident output distributions. In *International Conference on Learning Representations (ICLR)*, 2017. 2

[39] Alec Radford, Jong Wook Kim, Chris Hallacy, Aditya Ramesh, Gabriel Goh, Sandhini Agarwal, Girish Sastry, Amanda Askell, Pamela Mishkin, Jack Clark, Gretchen Krueger, and Ilya Sutskever. Learning transferable visual models from natural language supervision. In *International Conference on Machine Learning*, 2021. 1, 2, 3, 7

[40] Benjamin Recht, Rebecca Roelofs, Ludwig Schmidt, and Vaishaal Shankar. Do ImageNet classifiers generalize to ImageNet? In *Proceedings of the 36th International Conference on Machine Learning*, pages 5389–5400. PMLR, 2019. 5, 3

[41] Ashshak Sharifdeen, Muhammad Akhtar Munir, Sanoojan Baliah, Salman Khan, and Muhammad Haris Khan. O-TPT: Orthogonality constraints for calibrating test-time prompt tuning in vision-language models. In *Proceedings of the Computer Vision and Pattern Recognition Conference*, pages 19942–19951, 2025. 1, 2, 3, 4, 5, 6, 7

[42] Manli Shu, Weili Nie, De-An Huang, Zhiding Yu, Tom Goldstein, Anima Anandkumar, and Chaowei Xiao. Test-time prompt tuning for zero-shot generalization in vision-language models. *Advances in Neural Information Processing Systems*, 35:14274–14289, 2022. 1

[43] Julio Silva-Rodríguez, Fereshteh Shakeri, Houda Bahig, Jose Dolz, and Ismail Ben Ayed. Few-shot, now for real: Medical VLMs adaptation without balanced sets or validation. In *International Conference on Medical Image Computing and Computer-Assisted Intervention*, pages 237–247. Springer, 2025. 2

[44] Khurram Soomro, Amir Zamir, and Mubarak Shah. Ucf101: A dataset of 101 human actions classes from videos in the wild. *ArXiv*, abs/1212.0402, 2012. 5, 3

[45] Weijie Tu, Weijian Deng, Dylan Campbell, Stephen Gould, and Tom Gedeon. An empirical study into what matters for calibrating vision-language models. In *International Conference on Machine Learning*, pages 48791–48808. PMLR, 2024. 3

[46] Haohan Wang, Songwei Ge, Zachary Lipton, and Eric P Xing. Learning robust global representations by penalizing local predictive power. In *Advances in Neural Information Processing Systems*, pages 10506–10518, 2019. 5, 3

[47] Shuoyuan Wang, Jindong Wang, Guoqing Wang, Bob Zhang, Kaiyang Zhou, and Hongxin Wei. Open-vocabulary calibration for fine-tuned CLIP. In *International Conference on Machine Learning*, pages 51734–51754. PMLR, 2024. 3

[48] Jianxiong Xiao, James Hays, Krista A Ehinger, Aude Oliva, and Antonio Torralba. Sun database: Large-scale scene

recognition from abbey to zoo. In *IEEE Conference on Computer Vision and Pattern Recognition*, 2010. 5, 3

[49] Hu Xu, Saining Xie, Xiaoqing Tan, Po-Yao Huang, Russell Howes, Vasu Sharma, Shang-Wen Li, Gargi Ghosh, Luke Zettlemoyer, and Christoph Feichtenhofer. Demystifying CLIP data. In *The Twelfth International Conference on Learning Representations*, 2024. 1

[50] Jia-Qi Yang et al. Beyond probability partitions: Calibrating neural networks with semantic aware grouping. *Advances in Neural Information Processing Systems*, 36:58448–58460, 2023. 2

[51] Hee Suk Yoon, Eunseop Yoon, Joshua Tian Jin Tee, Mark A. Hasegawa-Johnson, Yingzhen Li, and Chang D. Yoo. C-TPT: Calibrated test-time prompt tuning for vision-language models via text feature dispersion. In *The Twelfth International Conference on Learning Representations*, 2024. 2, 3, 5

[52] Sangdoo Yun, Dongyoon Han, Seong Joon Oh, Sanghyuk Chun, Junsuk Choe, and Youngjoon Yoo. Cutmix: Regularization strategy to train strong classifiers with localizable features. In *Proceedings of the IEEE/CVF International Conference on Computer Vision (ICCV)*, pages 6023–6032, 2019. 2

[53] Hongyi Zhang, Moustapha Cisse, Yann N. Dauphin, and David Lopez-Paz. mixup: Beyond empirical risk minimization. In *International Conference on Learning Representations (ICLR)*, 2018. 2

[54] Jize Zhang et al. Mix-n-match: Ensemble and compositional methods for uncertainty calibration in deep learning. In *International conference on machine learning (ICML)*, 2020. 2

[55] Kaiyang Zhou, Jingkang Yang, Chen Change Loy, and Ziwei Liu. Conditional prompt learning for vision-language models. In *IEEE/CVF Conference on Computer Vision and Pattern Recognition (CVPR)*, 2022. 2

[56] Kaiyang Zhou, Jingkang Yang, Chen Change Loy, and Ziwei Liu. Learning to prompt for vision-language models. *International Journal of Computer Vision (IJCV)*, 2022. 2, 7, 3

SoC: Semantic Orthogonal Calibration for Test-Time Prompt Tuning

Supplementary Material

A. Proof of Proposition 1

We first note that for any \mathbf{v} and $i^* = \arg \max_i z_i$, the confidence can be written as

$$\begin{aligned} p_{\max}(\mathbf{v}) &= \frac{\exp(z_{i^*})}{\sum_{k=1}^K \exp(z_k)} \\ &= \frac{1}{1 + \sum_{j \neq i^*} \exp(z_j - z_{i^*})} \\ &= \frac{1}{1 + \sum_{j \neq i^*} \exp(-\Delta z_{i^* j}(\mathbf{v}))}. \end{aligned}$$

To obtain a universal bound, consider \mathbf{v} aligned with \mathbf{t}_{i^*} so that $\mathbf{v}^\top \mathbf{t}_{i^*} = 1$ (i.e., worst). Then for any $j \neq i^*$,

$$\mathbf{v}^\top \mathbf{t}_j = \mathbf{t}_{i^*}^\top \mathbf{t}_j \leq \max_{j \neq i^*} \mathbf{t}_{i^*}^\top \mathbf{t}_j = \mu,$$

hence each logit gap satisfies

$$\Delta z_{i^* j}(\mathbf{v}) = \alpha(\mathbf{v}^\top \mathbf{t}_{i^*} - \mathbf{v}^\top \mathbf{t}_j) \geq \alpha(1 - \mu), \quad \forall j \neq i^*.$$

By monotonicity of the exponential,

$$\exp(-\Delta z_{i^* j}(\mathbf{v})) \leq \exp(-\alpha(1 - \mu)), \quad \forall j \neq i^*,$$

and summing over all $K - 1$ competitors,

$$\sum_{j \neq i^*} \exp(-\Delta z_{i^* j}(\mathbf{v})) \leq (K - 1) \exp(-\alpha(1 - \mu)).$$

Substituting into the confidence expression

$$\begin{aligned} p_{\max}(\mathbf{v}) &= \frac{1}{1 + \sum_{j \neq i^*} \exp(-\Delta z_{i^* j}(\mathbf{v}))} \\ &\geq \frac{1}{1 + (K - 1) \exp(-\alpha(1 - \mu))}. \end{aligned}$$

□

B. Exact Similarity Shifts

We derive in this section the exact similarity shifts without considering the dominant-pair approximation. Let us consider the exact gradients for both O-TPT [41] and the proposed Huber-based regularizer:

$$\nabla_{\mathbf{t}_i}^{\text{O-TPT}} = 2 \sum_{k \neq i} s_{ik} \mathbf{t}_k, \quad (5)$$

and

$$\nabla_{\mathbf{t}_i}^{\text{Huber}} = \sum_{k \neq i} g_\delta(s_{ik}) \mathbf{t}_k, \quad \text{where} \quad g_\delta(s) = \begin{cases} s, & s \leq \delta, \\ \delta, & s > \delta. \end{cases} \quad (6)$$

O-TPT [41]. Substituting (5) into (2):

$$\begin{aligned}
\Delta s_{ij}^{\text{O-TPT}} &\approx -\eta \left(\mathbf{t}_j^\top \cdot 2 \sum_{k \neq i} s_{ik} \mathbf{t}_k + \mathbf{t}_i^\top \cdot 2 \sum_{k \neq i} s_{jk} \mathbf{t}_k \right) \\
&\approx -2\eta \left(\sum_{k \neq i} s_{ik} \mathbf{t}_j^\top \mathbf{t}_k + \sum_{k \neq i} s_{jk} \mathbf{t}_i^\top \mathbf{t}_k \right) \\
&\approx -2\eta \left(\sum_{k \neq i} s_{ik} s_{jk} + \sum_{k \neq j} s_{jk} s_{ik} \right). \tag{7}
\end{aligned}$$

By the definition of matrix multiplication,

$$(SS)_{ij} = \sum_{k=1}^n S_{ik} S_{kj} = \sum_{k=1}^n s_{ik} s_{kj} = \sum_{k=1}^n s_{ik} s_{jk},$$

and

$$(SS)_{ji} = \sum_{k=1}^n s_{jk} s_{ik}.$$

If we enforce zero diagonal in the sums, (to match $k \neq i$ or $k \neq j$), as in our case, these identities still hold with the understanding that the diagonal entries do not contribute. Therefore,

$$\begin{aligned}
\sum_{k \neq i} s_{ik} s_{jk} &\equiv (SS)_{ij}, \\
\sum_{k \neq j} s_{jk} s_{ik} &\equiv (SS)_{ji}. \tag{8}
\end{aligned}$$

Plugging (8) into (7) yields

$$\Delta s_{ij}^{\text{O-TPT}} \approx -2\eta ((SS)_{ij} + (SS)_{ji})$$

Considering that S is symmetric, then $(SS)_{ij} = (SS)_{ji}$, and hence:

(9)

SoC (Our proposed Huber-based regularizer). Analogously, we can plug the gradient in Eq. (6) into Eq. (2):

$$\begin{aligned}
\Delta s_{ij}^{\text{Huber}} &\approx -\eta \left(\sum_{k \neq i} g_\delta(s_{ik}) t_j^\top t_k + \sum_{k \neq j} g_\delta(s_{jk}) t_i^\top t_k \right) \\
&\approx -\eta \left(\sum_{k \neq i} g_\delta(s_{ik}) s_{jk} + \sum_{k \neq j} g_\delta(s_{jk}) s_{ik} \right). \tag{10}
\end{aligned}$$

Let $G = g_\delta(S)$ be the element-wise application of the Huber gradient function to S , with $G_{ij} = g_\delta(s_{ij})$ and $G_{ii} = 0$. Then the expression

$$\sum_{k \neq i} g_\delta(s_{ik}) s_{jk} \quad \text{and} \quad \sum_{k \neq j} g_\delta(s_{jk}) s_{ik}$$

can be written as matrix products:

$$(GS)_{ij} = \sum_k G_{ik} S_{kj} = \sum_k g_\delta(s_{ik}) s_{jk},$$

and similarly for $(GS)_{ji}$. Thus, Eq. 10 becomes

$$\Delta s_{ij}^{\text{Huber}} \approx -\eta [(GS)_{ij} + (GS)_{ji}].$$

If S is symmetric, then $(GS)_{ij} = (GS)_{ji}$, yielding:

$$\Delta s_{ij}^{\text{Huber}} \approx -2\eta (GS)_{ij}. \tag{11}$$

Implications for confidence bounds. The exact similarity shift derived above provides the structural foundation for Corollary 1. Specifically, the matrix form (Eqs. (9) and (11))

$$\Delta s_{ij}^{\text{O-TPT}} \approx -4\eta(S^2)_{ij} \quad \text{vs.} \quad \Delta s_{ij}^{\text{Huber}} \approx -2\eta(GS)_{ij}$$

reveals that O-TPT applies stronger gradients to high-similarity regions, leading to a more pronounced reduction in worst-case similarity $\mu = \max_{i \neq j} s_{ij}$. Since the softmax confidence lower bound $p_{\max}(\mathbf{v})$ depends inversely on μ (see Proposition 1), the sharper contraction under O-TPT yields a strictly higher confidence bound. In other words, the stronger second-order structure of O-TPT translates directly into more confident predictions, especially in regimes where prototype overlap is high.

C. Datasets

As stated in the main paper, to ensure a comprehensive and comparable evaluation, we follow established practices in recent prompt tuning literature [27, 41, 51, 56], assessing our approach on 11 widely studied datasets spanning diverse visual domains. These datasets have been consistently adopted in prior works to probe generalization, domain sensitivity, and semantic diversity, making them a strong basis for evaluating prompt-based methods. Detailed dataset statistics and descriptions are provided in Table 5.

Table 5. **Description of the datasets.** Number of classes, number of images in the test set, and brief description of the type of images.

	Num. classes	Num. images	Description
ImageNet [5]	1,000	50,000	Large-scale dataset of natural images.
DTD [4]	47	1,692	Diverse visual textures.
Flowers102 [34]	102	2,463	Various species of flowers.
Food101 [2]	101	30,300	Popular foods from around the world.
SUN397 [48]	397	19,850	Scene recognition dataset.
FGVC Aircraft [26]	100	3,333	Images of aircrafts, classified by model.
OxfordPets [37]	37	3,669	Images of pets, classified by breed.
Caltech101 [17]	101	2,465	Natural images from everyday objects.
UCF101 [44]	101	3,783	Human action recognition.
EuroSAT [8]	10	8,100	Satellite images of different types of land use.
StanfordCars [16]	196	8,041	Cars classified by brand and model.
ImageNet-A [11]	200	7,500	Natural images, challenging for most classifiers.
ImageNet-v2 [40]	1,000	10,000	Resampled ImageNet test set to verify robustness.
ImageNet-R [10]	200	30,000	Artistic renditions of ImageNet classes.
ImageNet-Sketch [46]	1,000	50,889	Drawn images from the ImageNet classes.

D. Additional Implementation Details

We normalize the cosine similarities $\tilde{\mathbf{S}} = \frac{\mathbf{S} - \mathbf{S}_{\min}}{\mathbf{S}_{\max} - \mathbf{S}_{\min}}$, to account for dataset-dependent class correlations. We choose the margin δ to be the 20-th percentile of $\tilde{\mathbf{S}}$. We chose the value of the weight of the regularizer $\lambda = 30$ for all experiments, except for the distribution shift experiments, where, similarly to previous work [41], we choose a smaller value of $\lambda = 14$. In order to keep an optimal scaling factor across all datasets, we use $\lambda \frac{|\mathcal{L}_{\text{SAC}}|}{|\mathcal{L}_{\text{TPT}}|}$, ensuring a constant optimal value. For C-TPT [51] and O-TPT [41], we use the original values of λ reported in the original works. All experiments were performed on NVIDIA A100 GPUs with 80 GB of memory.

E. Additional Experiments

Stability to initialization. In Tab. 6, we apply C-TPT, O-TPT, and our method across six datasets on three seeds (we chose six datasets with relatively small size to reduce the compute load), and report the standard deviation of the reported accuracy and calibration error. The lower standard deviation of both metrics indicated that our method is more stable to random initializations.

Table 6. **Standard deviations across three seeds:** accuracy and ECE across 6 datasets compared with state-of-the-art.

	DTD	Flowers	Aircraft	Pets	Caltech	UCF101	Average
Acc.	C-TPT	0.12	0.29	0.38	0.09	0.18	0.08
	O-TPT	0.06	0.15	0.23	0.07	0.06	0.14
	SoC (Ours)	0.16	0.06	0.03	0.04	0.13	0.03
ECE	C-TPT	0.09	0.30	0.42	0.04	0.23	0.04
	O-TPT	0.15	0.20	0.20	0.13	0.22	0.08
	SoC (Ours)	0.15	0.04	0.07	0.14	0.17	0.22

Table 7. **Accuracy and calibration error of SoC using three different normalizations.** Average performed over eight datasets. $\tilde{S}_1 = \frac{S - S_{\min}}{S_{\max} - S_{\min}}$, $\tilde{S}_2 = \frac{S}{S_{\max}}$, and $\tilde{S}_3 = S - S_{\min}$.

	\tilde{S}_1	\tilde{S}_2	\tilde{S}_3
Accuracy	70.3	70.7	69.2
ECE	5.3	7.3	5.5

Normalization strategies Tab. 7 shows an ablation with three different normalizations for SoC, justifying our choice for the $\tilde{S} = \frac{S - S_{\min}}{S_{\max} - S_{\min}}$ normalization.

Computational efficiency. The computational complexity of our SoC implementation is $O(n^2)$, while O-TPT has $O(n^3)$ complexity, due to the Householder transform, where n is the number of classes. Tab. 8 shows the FLOPS of SoC and O-TPT for varying number of classes, which aligns with the lower computational complexity.

Table 8. **Computational efficiency for varying number of classes.** MFLOPS of O-TPT and SoC for number of classes ranging from the smallest number (EuroSAT) to the highest number (ImageNet). Values correspond to the computational efficiency of computing the $\mathcal{L}_{\text{O-TPT}}$ and \mathcal{L}_{SoC} losses (i.e. not including the \mathcal{L}_{TPT} term).

	10	100	1000
O-TPT	0.2	20.4	6537.0
SoC (Ours)	0.2	15.4	1536.0

Detailed results. Tab. 9 shows the per-dataset results corresponding to the two-step updates shown in Fig. 4. The gaps in calibration error between SoC and O-TPT become very apparent, with certain datasets showing differences in ECE of 10.1 (DTD) and 26.1 (EuroSAT). Tab. 10 shows the per-dataset results of applying SaLS [33] on top of C-TPT, O-TPT, and SoC (Fig. 7). Because SaLS only scales the logits, the accuracy of the methods does not change, but the calibration error drops across all methods. As expected, as the models get better calibrated, the gap between methods is reduced.

Reliability plots. Fig. 9 and Fig. 10 shows the reliability plots across all datasets for O-TPT [41] and SoC, respectively. While EuroSAT is the most notable example, where calibration errors mostly vanish from O-TPT to SoC, the difference in calibration can also clearly be seen from the reliability plots in other datasets such as DTD, Flowers102, Aircraft, and UCF101. Analyzing the plots across all datasets confirms the overall tendency of O-TPT to be overconfident on its predictions.

Adaptive calibration error. The adaptive calibration error (ACE) is an alternative metric to the ECE, which defines the bins to not be equally spaced (as in ECE), but to all contain the same number of samples. Formally, the number of samples in each bin $n_i = \frac{M}{|B|}, \forall i \in \{1, \dots, |B|\}$, where M is the size of the test set, and B represents the bins. Tab. 11 shows the results of the ACE corresponding to the ViT-L/14 (i.e. an extension of Tab. 1).

Ablation on λ . The weight λ impacts the importance given to the regularization term relative to the TPT loss term, and acts as a tradeoff between the accuracy and the calibration. Higher values of λ will give more importance to the calibration, whereas lower values will favor better accuracy. Fig. 8 shows how the model performs in the accuracy-calibration space for different values of λ ranging from 10 to 50. Most points live in the lower-right side of O-TPT indicating better calibration and accuracy regardless of the chosen value of λ .

Table 9. **Applying two gradient updates.** Accuracy and ECE across 11 datasets compared with two baseline methods, when applying two gradient updates. Green and red indicate positive and negative changes with respect to O-TPT respectively.

	ImgNet	DTD	Flowers	Food101	SUN397	Aircraft	Pets	Caltech	UCF101	EuroSAT	Cars	Average
Acc.	C-TPT	75.2	54.4	76.5	89.0	70.7	30.0	94.1	95.4	74.8	50.7	76.5
	O-TPT	72.8	54.1	76.0	88.7	69.0	27.5	93.2	95.4	73.9	50.2	77.1
	SoC (Ours)	72.0_{1.4}	55.6_{+1.5}	77.9_{+1.9}	88.9_{+0.2}	70.1_{+1.1}	27.7_{+0.2}	94.1_{+0.9}	95.7_{+2.0}	75.9_{+5.2}	55.4_{-0.7}	76.4_{+1.4}
ECE	C-TPT	14.4	26.6	13.3	4.7	18.8	28.9	1.0	2.0	16.1	29.2	2.6
	O-TPT	7.8	21.2	8.6	3.9	10.0	22.8	0.9	1.1	11.5	29.5	1.4
	SoC (Ours)	10.3_{+2.5}	11.1_{-10.1}	6.6_{-2.0}	2.0_{-1.9}	8.0_{-2.0}	20.8_{-2.0}	1.1_{+0.2}	1.1_{-0.0}	6.8_{-4.7}	3.4_{-26.1}	1.4_{-0.0}

Table 10. **Applying SaLS [33] on ViT-L/14 backbone.** Accuracy and ECE across 11 datasets compared with two baseline methods, when applying SaLS on top of the TPT-based method. Green and red indicate positive and negative changes with respect to O-TPT respectively.

	ImgNet	DTD	Flowers	Food101	SUN397	Aircraft	Pets	Caltech	UCF101	EuroSAT	Cars	Average
Acc.	C-TPT	75.0	55.1	76.5	88.9	70.1	30.9	94.1	95.5	75.2	54.0	77.5
	O-TPT	73.2	54.6	76.4	88.6	68.9	30.0	93.8	95.3	74.5	53.6	76.7
	SoC (Ours)	74.5_{+1.3}	54.4_{-0.2}	77.0_{+0.6}	88.9_{+0.3}	69.5_{+0.6}	30.9_{+0.9}	93.9_{+0.1}	95.6_{+0.3}	74.9_{+0.4}	58.3_{+4.7}	77.0_{+0.3}
ECE	C-TPT	8.1	13.7	9.1	1.5	8.8	17.9	1.6	1.6	8.7	13.4	2.2
	O-TPT	3.8	9.9	5.4	1.5	3.6	13.6	2.1	2.7	6.2	13.7	3.6
	SoC (Ours)	6.1_{+2.3}	9.8_{-0.1}	4.7_{-0.7}	1.6_{+0.1}	5.1_{+1.5}	12.2_{-1.4}	1.2_{-0.9}	1.8_{-0.9}	5.6_{-0.6}	3.4_{-10.3}	2.8_{-0.8}

Table 11. **Adaptive calibration error on ViT-L/14.** ACE across 11 datasets compared with other baseline methods. Green and red indicate positive and negative changes with respect to O-TPT respectively.

	ImgNet	DTD	Flowers	Food101	SUN397	Aircraft	Pets	Caltech	UCF101	EuroSAT	Cars	Average
ACE	Zero-shot	2.9	10.2	4.5	1.7	3.3	10.3	2.4	3.7	5.7	7.2	3.9
	TPT	14.8	24.8	15.0	6.2	17.1	28.8	3.5	2.3	17.6	25.8	7.1
	C-TPT	10.5	18.3	11.1	3.3	13.4	21.4	1.0	0.9	11.1	17.3	1.4
	O-TPT	5.5	13.7	7.2	2.8	7.5	16.8	1.2	1.2	8.5	17.8	2.2
SoC (Ours)	7.2_{+1.7}	10.9_{+2.8}	5.5_{+1.7}	1.9_{+0.9}	7.1_{+0.4}	12.7_{+4.1}	0.5_{+0.7}	1.5_{-0.3}	6.3_{+2.2}	3.5_{+14.3}	2.2_{+0.0}	5.4_{-2.3}

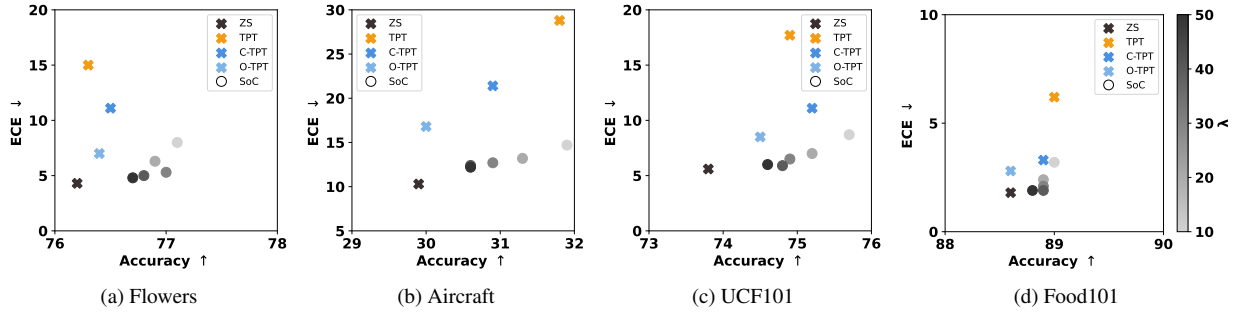


Figure 8. **Ablation on the value of λ .** Accuracy and calibration error for multiple values of the regularization term λ of SoC for the Flowers, Aircraft, UCF101, and Food101 datasets.

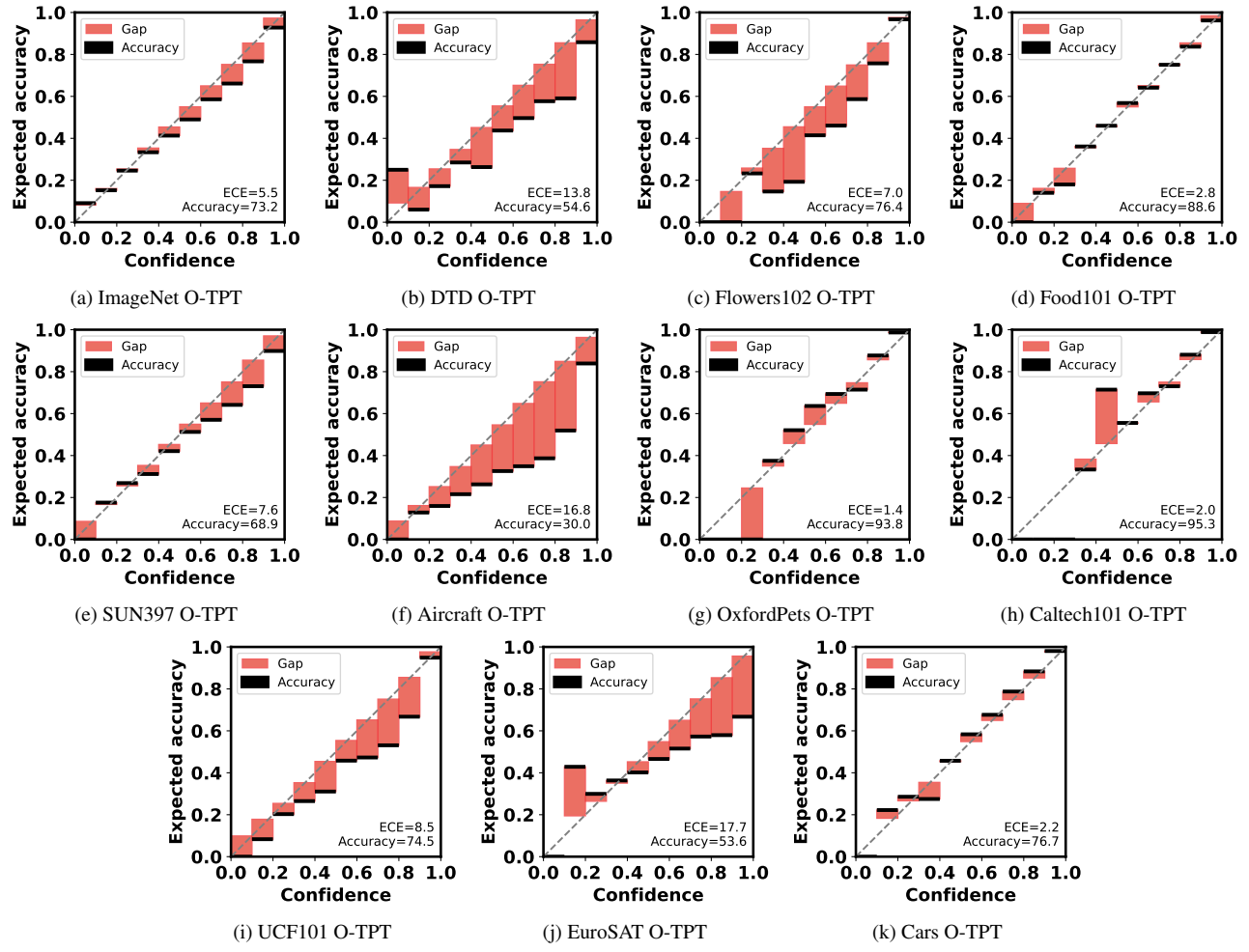


Figure 9. **Reliability plots for O-TPT.** Calibration error across all 11 datasets for O-TPT.

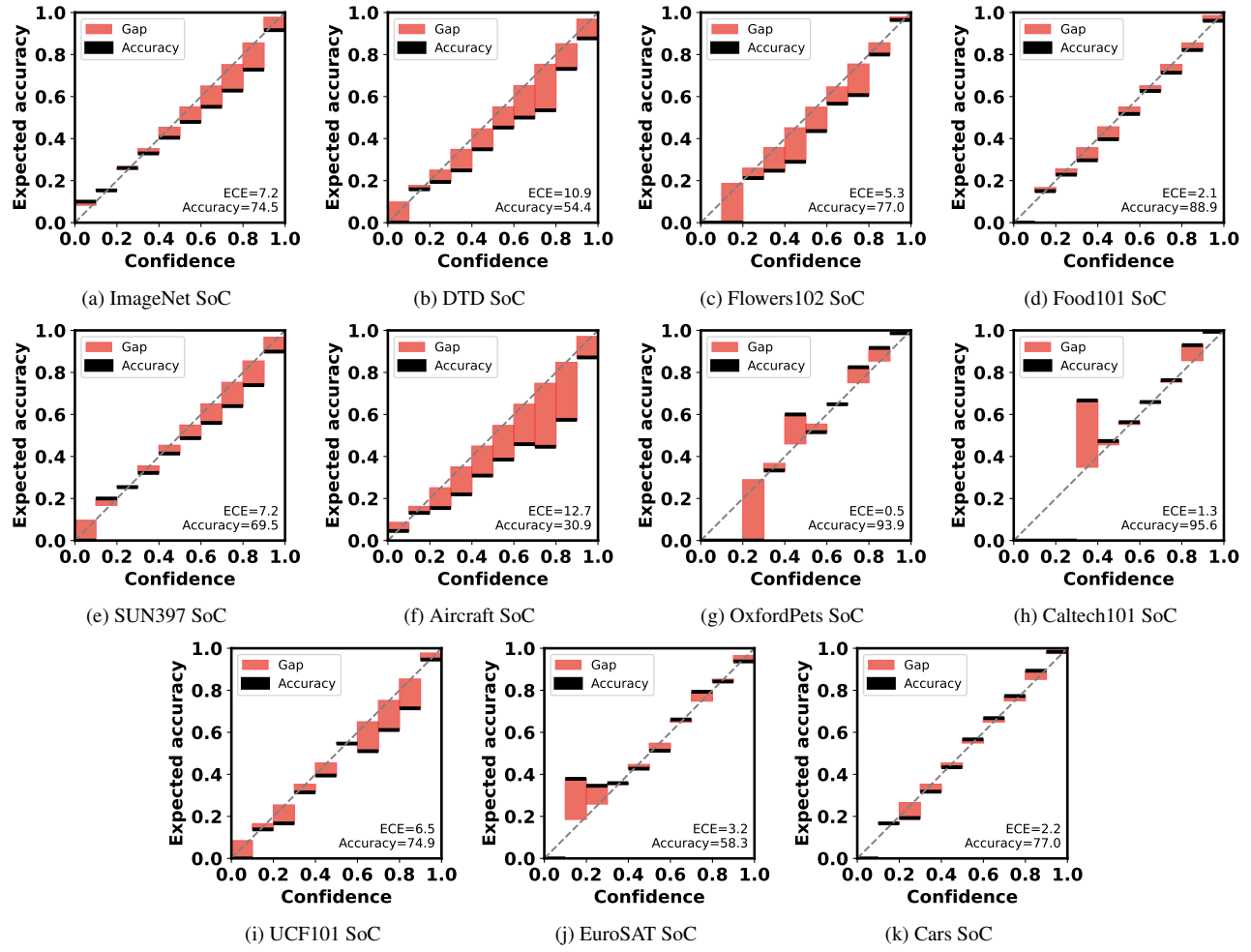


Figure 10. **Reliability plots for SoC.** Calibration error across all 11 datasets for SoC.